Cephalalgia

An International Journal of Headache

International Headache Society

Early-onset familial hemiplegic migraine due to a novel *SCN1A* mutation

Chunxiang Fan[1], Stefan Wolking[2], Frank Lehmann-Horn[1], Ulrike BS Hedrich[2], Tobias Freilinger[2], Holger Lerche[2], Guntram Borck[3], Christian Kubisch[4] and Karin Jurkat-Rott[1]

Abstract

Introduction: Familial hemiplegic migraine (FHM) is a rare autosomal dominant subtype of migraine with aura. The FHM3 subtype is caused by mutations in *SCN1A*, which is also the most frequent epilepsy gene encoding the voltage-gated Na^+ channel $Na_V1.1$. The aim of this study was to explore the clinical, genetic and pathogenetic features of a pure FHM3 family.

Methods: A three-generation family was enrolled in this study for genetic testing and assessment of clinical features. Whole cell patch-clamp was performed to determine the functions of identified mutant $Na_V1.1$ channels, which were transiently expressed in human tsA201 cells together with β_1 and β_2 subunits.

Results and conclusions: We identified a novel *SCN1A* (p.Leu1624Pro) mutation in a pure FHM family with notably early-onset attacks at mean age of 7. L1624P locates in S3 of domain IV, the same domain as two of four known pure FHM3 mutations. Compared to WT channels, L1624P displayed an increased threshold-near persistent current in addition to other gain-of-function features such as: a slowing of fast inactivation, a positive shift in steady-state inactivation, a faster recovery and higher channel availability during repetitive stimulation. Similar to the known FHM3 mutations, this novel mutation predicts hyperexcitability of GABAergic inhibitory neurons.

Keywords

Familial hemiplegic migraine, early-onset, gain of function, FHM3, $Na_V1.1$

Date received: 15 May 2015; revised: 27 July 2015; accepted: 29 August 2015

Introduction

Familial hemiplegic migraine (FHM) is a rare autosomal dominant migraine subtype associated with aura including reversible hemiparesis (1,2). FHM has a remarkable phenotypic variability among patients even within the same family. Clinical onset is usually during youth. So far three causative genes have been identified, all encoding ion transport proteins: *CACNA1A* (FHM1) (3), *ATP1A2* (FHM2) (4) and *SCN1A* (FHM3) (5). Recently *PRRT2* has also been found to be associated with hemiplegic migraine (6). Mutations in these four genes are postulated to influence the initiation and propagation of cortical spreading depression (CSD), as evidenced by data from gene-targeted mouse models. CSD is a short-lasting propagating wave of cellular depolarization followed by a long-lasting suppression of the neuronal activity that is believed to be the basis for the migraine aura (7). The likelihood of CSD is increased by hyperexcitability

of the neuronal network (8,9). In FHM1, $Ca_V2.1$ mutations induce a gain-of-function resulting in enhanced glutamate release and facilitated CSD. In FHM2, mutations of the sodium potassium ATPase cause a loss of function, leading to accumulation of extracellular K^+ and the development of CSD (8,9). In FHM3, $Na_V1.1$ mutations predict increased firing and a

[1]Division of Neurophysiology, Ulm University, Germany
[2]Department of Neurology and Epileptology, Hertie Institute for Clinical Brain Research, University of Tübingen, Germany
[3]Institute of Human Genetics, Ulm University, Germany
[4]Institute of Human Genetics, University Medical Center Hamburg-Eppendorf, Germany

Corresponding author:
Karin Jurkat-Rott, Division of Neurophysiology, Ulm University, Containerstadt Helmholtzstrasse 10/1, 89081 Ulm, Germany.
Email: Karin.jurkat-rott@uni-ulm.de

hyperexcitability of GABAergic neurons. This may also lead to an increase in extracellular K^+ and thereby trigger CSD (10,11).

SCN1A, the gene encoding $Na_V1.1$, is the most relevant gene in epilepsy with hundreds of mutations linked to a spectrum of epilepsy syndromes of varying severity (12). Previous studies of these epileptic mutations revealed mainly loss-of-function effects, particularly in mouse models. These studies predict network hyperexcitability due to specifically reduced action potential firing in inhibitory GABAergic interneurons, in which $Na_V1.1$ is predominantly expressed (13–15). In vitro studies, also mainly loss-of-function effects were found, whereas a few studies also reported partial gain-of-function effects (16). Until now, only eight *SCN1A* missense mutations have been described to cause FHM3. Of those, some mutations (Q1489K, L1649Q, I1498M and F1661L) were identified in pure FHM families (5,17,18), whereas others were described to be linked to FHM associated with either epileptic seizures (L263Q, T1174S and Q1489H) or elicited repetitive daily blindness (Q1489H and F1499L) (19–21). Functional investigation of FHM3-causing *SCN1A* mutations revealed that most had gain-of-function effects such as increased non-inactivated depolarization-induced persistent sodium currents, delayed entry into inactivation, accelerated recovery from fast inactivation and rescue of folding defects by incubation at lower temperature or co-expression of interacting proteins (5,10,11,17,22). In contrast, the FHM3 mutation T1174S in $Na_V1.1$, which incidentally caused a mixed FHM3 and epilepsy phenotype, showed both gain and loss of function (21).

In the present study, we identify a novel $Na_V1.1$ L1624P mutation in a pure FHM family with early age at clinical onset. Electrophysiological studies show an overall gain of function of this mutation in agreement with the previously assumed pathomechanism of FHM3.

Materials and methods

Genetics

A three-generation family with five FHM patients was enrolled in this study, and the clinical features were analyzed. Their blood samples were collected for mutation screening after informed consent was obtained. All procedures were approved by the Ethics Committee of Ulm University and were in accordance with the Declaration of Helsinki. The mutation screening was performed by direct sequencing of all coding exons and exon-intron junctions of *CACNA1A*, *ATP1A2* and *SCN1A* genes. *SCN1A* mutation nomenclature is based on reference transcript NM_001165963.1.

Functional studies

The shorter isoform (−11 amino acids) of the human $Na_V1.1$ α subunit subcloned to the pCDM8 vector was used for site-directed mutagenesis of L1613P (equivalent mutation L1624P). *SCN1A* was transiently transfected in human tsA201 cells together with the auxiliary subunits β1 and β2 coupled to green fluorescent protein (GFP) and CD8 antigen, respectively. Whole-cell patch clamp recordings were performed 24 hours after transfection. Only cells expressing both reporters and producing voltage-dependent inward sodium currents as previously reported were used and analyzed (23). The pipette resistance was around $1.5\,M\Omega$ after filling with internal solution containing (in mM): NaF 10, CsF 110, CsCl 20, ethylene glycol tetraacetic acid (EGTA) 2, HEPES 10, NaATP 2 and NaGTP 0.2. The external solution contained (in mM) NaCl 145, KCl 4, $CaCl_2$ 1.8, $MgCl_2$ 1 and HEPES 10. pH was adjusted to 7.3 and osmolarity to ∼300 mOsm. Before data acquisition, cells were allowed to stabilize for 10 min after establishment of the whole-cell configuration. Sodium currents were recorded at room temperature (21–23°C) after partial series resistance compensation (∼85%) using an Axopatch 200B amplifier (Axon Instruments). The voltage errors were <5 mV. Data were filtered at 10 kHz and sampled at 50 kHz. Only amplitudes of peak sodium currents between 1.3 to 14 nA were used for analysis. All recordings were performed without online leak subtraction. The linear passive currents at various potentials were calculated from the value at the holding potential of −120 mV, and these currents were subtracted from the current recordings.

Data analysis

The steady-state activation was determined by fitting the peak current-voltage relation with the equation

$$I = g_{max} \times (V - V_{rev})/(1 + \exp((V_{0.5} - V)/k))$$

with V_{rev} and g_{max} being the reversal potential and maximum conductance of channels, $V_{0.5}$ the potential for half-maximal current, V the test potential and k the slope factor.

Time constants of fast inactivation were obtained by fitting a double exponential function to the current decay

$$t = A_{fast} * \exp(-t/\tau_{fast}) + A_{slow} * \exp(-t/\tau_{slow}) + C$$

with t being the time, A_{fast} and A_{slow} the fraction of channels inactivating with time constant τ_{fast} and τ_{slow}, respectively, and C the asymptote.

Steady-state inactivation curves were evaluated by fitting the data to the equation

$$I/I_{max} = A/(1 + \exp((V_{0.5} - V)/k)) + C$$

with V representing the pre-pulse potential, $V_{0.5}$ the potential at which half of the channels are inactivated, C the fraction of non-inactivated channels and k is the slope factor.

The recovery from inactivation was analyzed by fitting the data with a double exponential function:

$$I/I_{max} = A_{fast} * (1 - \exp(-t/\tau_{fast}))$$
$$+ A_{slow} * (1 - \exp(-t/\tau_{slow})) + C$$

with τ_{fast} and τ_{slow} denoting a fast and a slow time constant, A_{fast} and A_{slow} representing the two fractional amplitudes and C the level of non-inactivating sodium current.

Entry into slow inactivation was fitted by a single decay function

$$I/I_{max} = A * \exp(-t/\tau) + C$$

with t being the time, A the fraction of channels inactivating with time constant τ and C the asymptote.

Data were analyzed by a combination of pClamp (Axon Instruments), Excel (Microsoft), SPSS (IBM) and ORIGIN (MicroCal software). Data are presented as mean $\pm$ standard error of the mean (SEM). Student's t-tests were applied for statistical evaluation with significance levels set to $*p < 0.05$, $**p < 0.01$ and $***p < 0.001$.

Results

Phenotype and genotype

The three-generation German family contained five patients with migraine attacks fulfilling International Headache Society (IHS) criteria for FHM (Figure 1(a)). All patients, except the deceased grandfather of the index patient, underwent a detailed semi-structured individual personal interview or telephone interview, putting particular emphasis on the occurrence and severity of motor aura symptoms. Detailed clinical characteristics are depicted in Table 1.

III.1 The index patient, currently 27 years of age, had hemiplegic migraine since the age of 5. Attacks occurred once or twice per month. Hemiplegia started usually in the upper limb with spreading to the lower limb causing inability to walk or hold objects. Scintillating scotoma, unilateral numbness and moderate aphasia often preceded hemiplegia. The hemiplegic attacks usually lasted for several hours, overlapping with the occurrence of ipsilateral or contralateral migrainous headache. After puberty attacks became less frequent ($1–2\times$/year) and less severe. Cerebral magnetic resonance imaging (MRI) with contrast enhancement was normal and repeated electroencephalograms (EEGs), including 24-hour EEG and sleep-deprivation EEG, showed no epileptic features.

II.2 The index patient's mother, currently 58 years of age, had hemiplegic migraine since the age of 8. She reported attacks two to three times/year. Hemiplegia occurred simultaneously in the upper and lower limb with clear preponderance of the right side. Scintillating scotoma and paresthesia could regularly precede hemiplegia. Aura symptoms usually lasted for several hours, followed by ipsilateral migrainous headache. After puberty the attacks became milder and less frequent. Migraine without aura occurred once a month. Cerebral MRI and repeated EEGs were normal.

II.3 The index patient's uncle, currently 48 years of age, had hemiplegic migraine since the age of 8 years. He reported hemiplegic attacks several times per year. Hemiplegia was preceded by spreading visual and sensory aura as well as dysarthria. Aura symptoms persisted for 30 minutes, and after dissolution unilateral
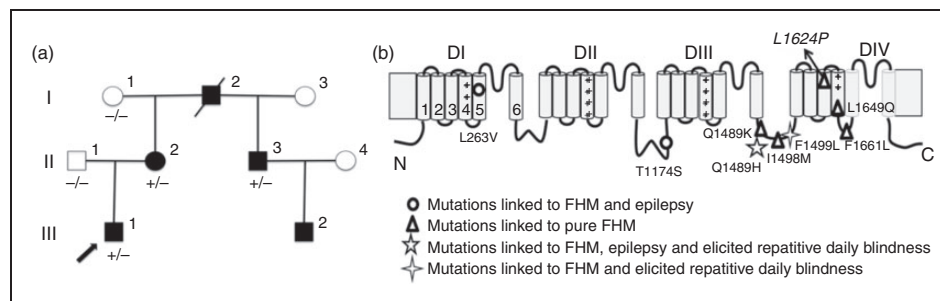
Figure 1. FHM family with a novel *SCN1A*-L1624P mutation.
(a) Family pedigree. The proband is indicated by an arrow. III.2 did not attend the genetic test. Squares show men and circles women. Black inlays show affected and white healthy individuals. +/– refers to presence or absence of mutated *SCN1A* allele. (b) Scheme of the Na$_V$1.1 α subunit showing the location of the novel mutation L1624P indicated by arrow and known FHM3 mutations. FHM: familial hemiplegic migraine.

Table 1. Clinical features of the FHM3 family.

ID	Age (years)	HM onset (years)	Triggering factors for hemiplegic attacks	Aura symptoms during hemiplegic attacks					Hemiplegic attacks			Headache characteristics					Nausea/ vomiting/ photophobia/ phonophobia	Other types of attacks
				H	S	V	A	Others	Duration	Frequency	Side	Duration	Side	Character	Temporal relation to hemiplegic attacks	Anatomical relation to hemiplegic attacks		
I.2	[a]	NK	–	+	+	NK	NK	–	NK	NK	NK	NK	NK	NK	NK	NK	NK	NK
II.2	58	8	Emotional stress	+	+	+	–	Panic	30 minutes to three hours	2–3/year	R > L	Up to six hours	Unilateral	Piercing	HP > HA	Ipsilateral	–/–/–/–	MO
II.3	48	8	–	+	+	+	+	Dysarthria	30 minutes	3–4/year	R = L	Up to 24 hours	Uni- and bilateral	Pressing	HP > HA	Ipsilateral	–/–/–/+	Isolated visual aura
III.1	27	5	Nutrients: walnuts, aspartame, cheese	+	+	+	+	–	15 minutes to 12 hours	1–2/month	R < L	Up to 12 hours	Unilateral	Stabbing, throbbing	HP > HA	Ipsi- and contralateral	+/+/+/+	Isolated hemiplegic aura
III.2	10	6	–	+	+	+	+	–	20 minutes	3/year	R = L	Up to 24 hours	Bilateral	Pressing	HP > HA	NA	–/–/–/+	–

aDeceased. ID: identification; FHM3: familial hemiplegic migraine 3; NK: not known; NA: not applicable; H: hemiplegic; S: sensory disturbance; V: visual disturbance; A: aphasia; MO: migraine without aura; HP > HA: hemiplegic attack precedes headache; R: right side; L: left side.

or bilateral headache followed. On rare occasions isolated visual aura occurred. Cerebral MRI and repetitive EEGs were normal.

III.2 The son of II.3 started having similar attacks at the age of 6 years. He is now 10 years old. Hemiplegia was preceded by visual and sensory aura and dysarthria and persisted for 20 to 30 minutes. Headache occurred after migraine dissolution.

I.2 The grandfather was deceased at the time of the interview. According to the family members, he suffered from hemiplegic migraine attacks that were reported as very similar to the phenotype of II.2.

All four tested affected family members (I.2, II.2, II.3, III.1) harbor a heterozygous T to C substitution at nucleotide 4871, corresponding to an L1624P mutation in segment S3 of domain IV of $Na_V1.1$ (Figure 1(b)). This variant has not been reported in >120,000 alleles included in the ExAC browser. No mutations were detected in *CACNA1A* and *ATP1A2* genes. III.2 did not attend the genetic test.

Electrophysiology

Representative whole-cell currents recorded from tsA201 cells expressing wild-type (WT) or mutant channels were elicited by various test potentials from a holding potential of −120 mV (Figure 2(a)). Peak current density of the mutant channels was similar to that of the WT channels (L1624P: −391.11 ± 56.46 pA/pF vs WT: −401.88 ± 47.93 pA/pF, Figure 2(a)). Likewise, voltage dependence of activation revealed no significant difference between WT ($V_{0.5} = -23.93 \pm 1.18$ mV) and mutant L1624P channels ($V_{0.5} = -25.36 \pm 1.04$ mV). The time course of fast inactivation was fitted to a second-order exponential function with currents being elicited by test pulses between −40 and 20 mV. There was a significant slowing of mutant channels, especially of the fast component (Figure 2(b)); i.e. at a test potential of −10 mV eliciting the maximum peak current, τ_{fast} of the mutant L1624P (1.21 ± 0.09 ms) was around 2.4 times slower than that of WT channels (0.52 ± 0.02 ms). This finding suggests a destabilization of the inactivated state of $Na_V1.1$ channels. In agreement with this hypothesis, mutant channels showed a significant depolarizing shift of the steady-state fast inactivation curve ($V_{0.5} = -49.10 \pm 1.18$ mV) compared with WT $Na_V1.1$ channels ($V_{0.5} = -58.29 \pm 1.17$ mV) (Table 2).

To investigate the recovery from inactivation states, cells were depolarized to −10 mV for 100 ms to inactivate Na^+ channels and then repolarized to −120 mV recovery potential for increasing
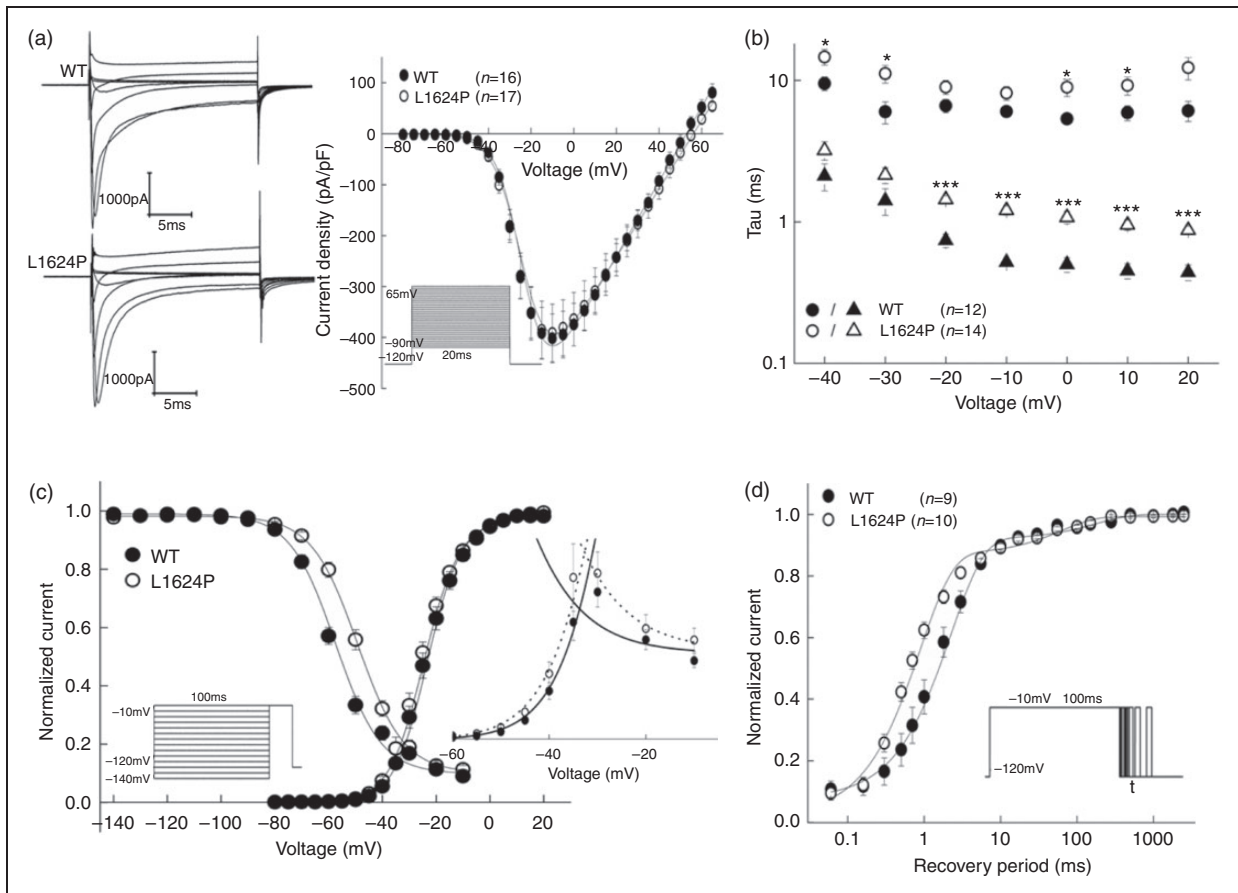
Figure 2. Functional characteristics of WT (filled symbols) and mutant L1624P (open symbols) channels expressed in tsA201 cells. (a) Averaged whole-cell currents of WT and mutant channels elicited from a holding potential of −120 mV by voltage steps between −80 and +65 mV in 5 mV intervals for 20 ms. For clarification, the currents were shown every 20 mV. (b) Voltage-dependence of both fast and slow time constants of fast inactivation of WT and mutant channels. (c) Steady-state fast inactivation curves (WT: $n = 16$ vs L1624P: $n = 22$) and conductance − voltage curves. Inactivation curves were determined from a holding potential of −120 mV using a series of 100 ms prepulses to potentials between −140 and −10 mV in 10 mV steps followed by a −10 mV test pulse. An overlay of WT and L1624P window currents are shown in inset. (d) Recovery from inactivation with a two-pulse protocol: a 100 ms-lasting depolarization prepulse to −10 mV was used to inactivate sodium channels, a second −10 mV test pulse followed after an increasing interval from 0.06 to 2500 ms from a holding potential of −120 mV. Protocols are shown in insets. Data are shown as means ± SEM. Lines are fits to corresponding equations given in the text. Fitting parameters are listed in Table 2. Significance levels were set to *$p < 0.05$, ***$p < 0.001$. WT: wild-type.

duration (Figure 2(d), inset). Its time course was well fit to a second-order exponential function, yielding two time constants, τ_{fast} and τ_{slow} (Figure 2(d)). The faster time constant τ_{fast} was significantly decreased for mutant compared with WT channels, whereas the slower component τ_{slow} was similar between WT and mutant channels. For the fast component, the mutant channels recover two times faster than WT channels. All gating parameters are listed in Table 2.

As a result of the depolarizing shift of steady-state inactivation, the window currents of mutant L1624P channels were increased by 27.73% (Figure 2(c) inset). Therefore, we expected an increase of persistent sodium currents. To test this hypothesis, we examined currents

that were elicited by 100 ms depolarizing pulses between −40 and 10 mV (in 10 mV increments) and calculated the ratio of the non-inactivating current, which could be blocked by tetrodotoxin (TTX) (data not shown), and the peak transient sodium current at various potentials (Figure 3 inset). We found a significant increase of this ratio for test potentials near threshold of an action potential in cells expressing mutant L1624P channels (0.17 ± 0.02) compared with WT-expressing cells (0.08 ± 0.03) (Figure 3). Altogether, these results of an increased window and persistent current as well as an accelerated recovery from fast inactivation indicate a gain of function and predict an increase in neuronal excitability via depolarization of the membrane and a

Table 2. Gating parameters of WT and mutant channels.

Parameters	WT	L1624P
Parameters for fast kinetics		
Voltage dependence of activation	$n = 16$	$n = 17$
Peak current density (pA)	-401.88 ± 47.93	-391.11 ± 56.46
Capacitance (pF)	10.73 ± 0.64	9.95 ± 0.68
V_{rev} (mV)	53.81 ± 1.64	54.77 ± 1.53
$V_{0.5}$ (mV)	-23.93 ± 1.18	-25.36 ± 1.04
k	5.84 ± 0.27	5.95 ± 0.31
Voltage dependence of inactivation	$n = 16$	$n = 22$
$V_{0.5}$ (mV)	-58.29 ± 1.17	-49.10 ± 1.18[a]
k	-8.28 ± 0.89	-7.98 ± 0.47
Recovery from fast inactivation	$n = 9$	$n = 10$
τ_{fast} (ms)	1.86 ± 0.38	0.79 ± 0.07*
τ_{slow} (ms)	55.0 ± 21	36.7 ± 8.01
Parameters for slow kinetics		
Entry into slow inactivation	$n = 6$	$n = 5$
τ	3768.9 ± 729.1	2458.3 ± 237.9
Steady-state slow inactivation	$n = 9$	$n = 7$
$V_{0.5}$ (mV)	-51.68 ± 2.02	-51.57 ± 2.38
k	-7.42 ± 0.32	-5.30 ± 0.09[a]
Recovery from slow inactivation	$n = 4$	$n = 5$
τ_{fast} (ms)	76.48 ± 39.95	114.19 ± 19.60
τ_{slow} (ms)	982.73 ± 403.86	1855.32 ± 538.69

Significance levels were set to *$p < 0.05$, [a]$p < 0.001$.
WT: wild-type.

shortening of the refractory period after an action potential.

We also tested the slow inactivation properties both for WT and mutant channels (Figure 4). Entry into slow inactivation was monoexponential, with a time constant around 3000 ms for both WT and L1624P channels without significant difference (Table 2). There was no voltage shift of steady-state slow inactivation for L1624P compared to WT, while the slow inactivation voltage sensitivity was significantly different (Table 2). Both WT and L1624P recover in a biexponential way from slow inactivation without significant differences (Table 2). Compared to WT, the slow inactivation properties of L1624P almost remained unchanged.

To simulate the channel availability during neuronal firing, we recorded the so-called use-dependence, i.e. whole-cell peak currents during 300 repetitive depolarizing voltage steps to −10 mV at different frequencies and from different holding potentials (Figure 5). At the holding potential of −120 mV, there was no significant difference between the availability of WT and L1624P channels, with both maintaining high channel availability. However, at holding potentials in the physiological range (i.e. more depolarized), mutant channels exhibited a significantly higher availability compared with WT channels. Especially around the neuronal resting membrane potential of −70 mV and a stimulation frequency of 100 Hz (Figure 5), the residual channel availability of mutant L1624P channels was 0.64 ± 0.03, almost twofold higher than for WT channels (0.33 ± 0.03), indicating a marked gain of function in the physiologically relevant range (Table 3). Altogether, our functional studies show a clear gain-of-function effect for mutant $Na_V1.1$ in comparison to WT channels.

Discussion

Here we report a German family with pure FHM. In detail, there is a high intra-individual clinical variability with respect to attack duration, severity and frequency. Maybe the most notable clinical feature is that all patients were found to have an early onset of the attacks before puberty (mean age 7 (range 5 to 8) compared to a mean age of 13 in other reported FHM3
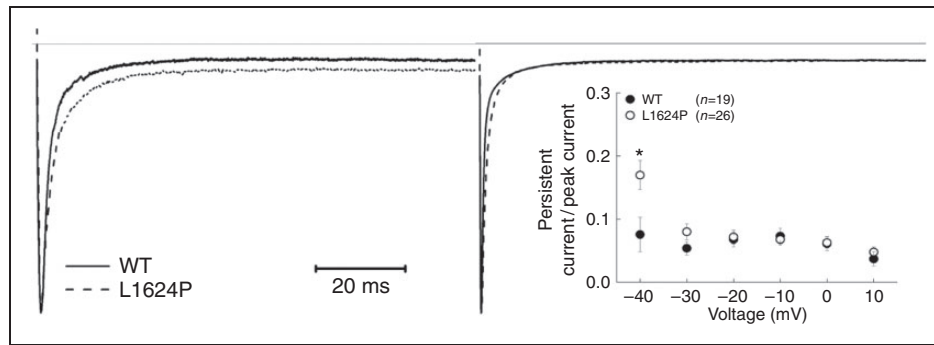
Figure 3. Persistent sodium currents of WT and mutant L1624P channels.
Sodium currents were elicited by a 100 ms-long depolarizing pulse to −40 (left traces) or −10 mV (right traces) from a holding potential of −120 mV. The upper line indicates the zero line. Each trace was normalized to the peak of the transient sodium current. Percentage of persistent current to peak current responding to various depolarization pulses (from −40 to −10 mV) is given in the inset. Data are shown as means ± SEM. Significance levels were set to *$p < 0.05$.
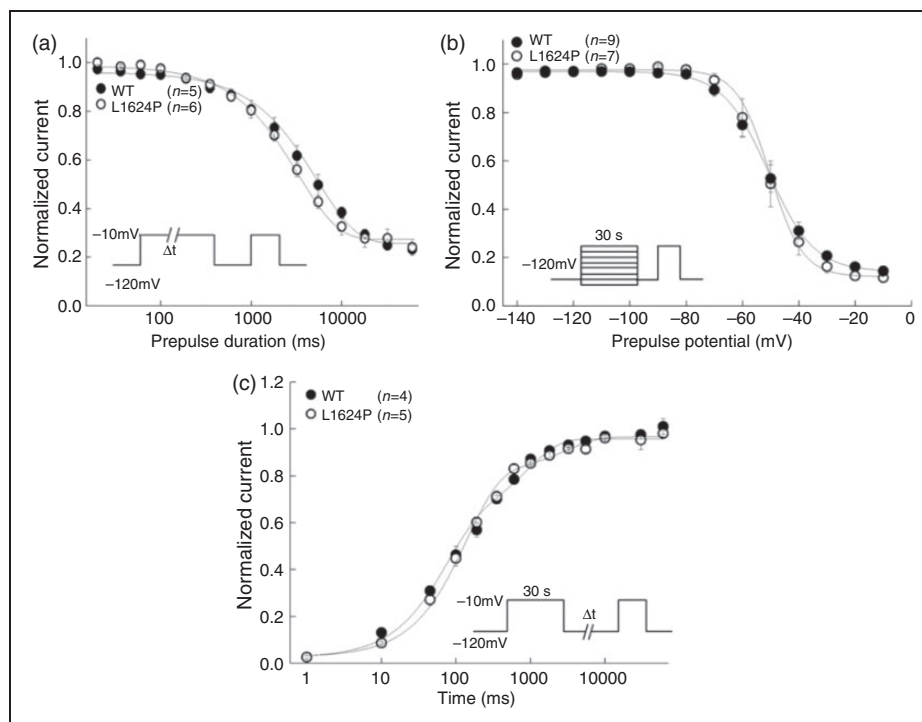
Figure 4. Slow inactivation properties of WT (filled circles) and mutant L1624P (open circles).
(a) Entry into slow inactivation was elicited from a holding potential of −120 mV by a depolarizing pulse to −10 mV for an increasing time period (0.02−60 s). An interval of 50 ms at −120 mV followed to recover the fast inactivated but not slow inactivated channels. Then the fraction of slow inactivated channels was determined by the following 20 ms test pulse to −10 mV. Cells were held at −120 mV between trials for 30 s to allow the recovery from slow inactivation. (b) Steady-state slow inactivation was determined by a 30 s conditioning pulse between −140 to −10 mV, followed by a 50 ms recovery period at −120 mV prior to the −10 mV test pulse. The cumulative steady-state slow inactivation was performed with no recovery from slow inactivation between two trials. (c) Recovery from slow inactivation was measured by a 30 s depolarizing pulse to −10 mV followed by an increasing recovery duration (from 0.001 to 60 s) from holding potential of −120 mV. The test pulse to −10 mV was then employed to record the recovered sodium currents. Cells were held at −120 mV between trials for 30 s to allow the recovery from slow inactivation. Protocols are shown in insets. Data are shown as means ± SEM. Lines are fits to corresponding equations given in the text. Fitting parameters are listed in Table 2.
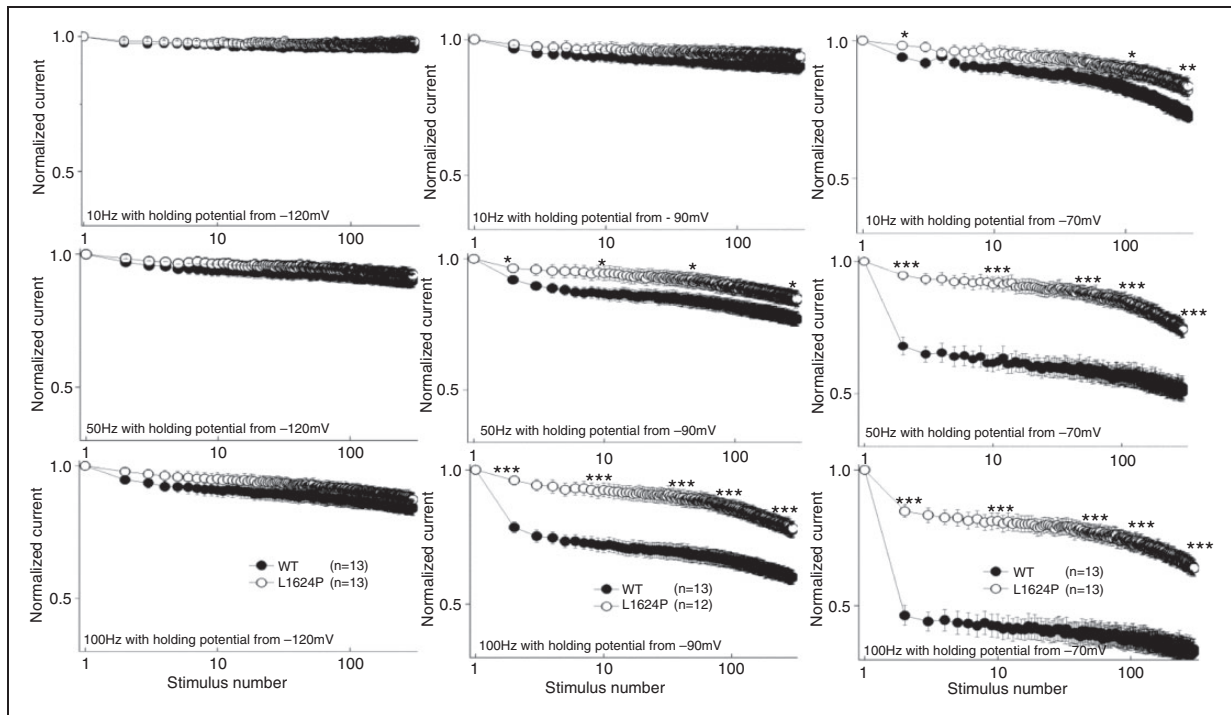
Figure 5. Use dependence of WT and mutant L1624P channels.
Currents were elicited by 300 consecutive trains of 2 ms-long depolarizing pulses to −10 mV from different holding potentials (−120 mV (left), −90 mV (middle) and −70 mV (right graphs)) at different frequencies (10 Hz (top graphs), 50 Hz (middle graphs) and 100 Hz (bottom graphs)). Each trace was normalized to the initial transient peak sodium current. Data are shown as means ± SEM. Significance tested for each fiftieth pulse were set to *$p < 0.05$, **$p < 0.01$, ***$p < 0.001$. WT: wild-type.

Table 3. Parameters of use dependence.

Parameter	WT	L1624P
Holding potential of −120 mV		
10 Hz	0.96 ± 0.01	0.98 ± 0.01
50 Hz	0.90 ± 0.02	0.92 ± 0.02
100 Hz	0.84 ± 0.03	0.87 ± 0.02
Holding potential of −90 mV		
10 Hz	0.90 ± 0.02	0.94 ± 0.03
50 Hz	0.77 ± 0.02	0.85 ± 0.03[a]
100 Hz	0.60 ± 0.02	0.78 ± 0.03[c]
Holding potential of −70 mV		
10 Hz	0.72 ± 0.02	0.83 ± 0.03[b]
50 Hz	0.52 ± 0.04	0.74 ± 0.03[c]
100 Hz	0.33 ± 0.03	0.64 ± 0.03[c]

Significance levels were set to [a]$p < 0.05$, [b]$p < 0.01$, [c]$p < 0.001$. WT: wild-type.

families (range 6 to 24) (24)). Permanent neurological disturbances that have been previously described for FHM1 and 2 families such as cognitive deficits (FHM1 and 2) or cerebellar dysfunction (FHM1) (25,26) were not observed. In addition, we did not observe elicited repetitive daily blindness, for which a partial cosegregation with FHM had been described in two French FHM3 pedigrees (19). The identified novel mutation, expanding the spectrum of FHM3 mutations by increasing their number to nine, is located in the S3 segment of domain IV, in the same domain as two of four known mutations causing pure FHM (F1661L and L1649Q). Until now, mutations causing pure FHM3 have been reported to affect this domain as well as the DIII/IV linker, whereas the others are located in different regions of the channel (see also Figure 1), therefore the novel L1624P mutation expands the spectrum of FHM3 mutations by increasing their number to nine. Other missense mutations in IV/S3 have been described causing different clinical phenotypes such as severe myoclonic epilepsy of infancy (SMEI), borderline SMEI (SMEB) or intractable childhood epilepsies with frequent generalized tonic-clonic seizures (27–30).

Functional studies of L1624P revealed a severe disturbance of fast inactivation with a slower inactivation time course, an 11-mV depolarizing shift of the steady-state inactivation curve, and a two times accelerated recovery from fast inactivation. These effects suggest a destabilization of the inactivated state. L1624P

substitutes a proline residue with a high turn propensity (31) for the hydrophobic, relatively long side-chain of leucine; L1624P therefore is likely to introduce a hinge in the S3 segment of domain IV distorting the regular structure of the segment (32). Segment IV/S3 has been shown to be involved in fast inactivation before (as, for example, suggested for the muscle sodium channel Na$_V$1.4; (33)). It is therefore conceivable that L1642P affects the channel's fast inactivation.

Also mutant L1624P channels displayed an abnormal threshold-near persistent current that might be due to the increased window current. This is different from the persistent current detected in other FHM3 mutations, which appear even at more depolarized potential ranges (11,21,22). This unusual persistent current near the threshold might also contribute to more sodium influx during the repolarizing phase of action potentials and facilitate the longer duration of action potentials leading to increased neuron excitability (21). Investigation of slow inactivation properties showed L1624P mostly unchanged, which indicates slow inactivation might not be involved in the pathogenesis of FHM.

All these results indicate a clear gain of function of mutant Na$_V$1.1 channels predicting increased availability and enhanced sodium influx. Furthermore, the higher availability maintained by mutant L1624P in use-dependence experiments suggests that neurons expressing L1624P mutant channels can sustain high-frequency firing better than cells expressing WT channels, or that cells with mutant channels can generate higher firing frequencies than neurons with only WT channels. This is in agreement with most previous results of functional studies of FHM3 mutations (5,11,17,22) and strengthens the main hypothesis, that gain-of-function mutations in the *SCN1A* gene cause FHM3. As Na$_V$1.1 is the predominant channel in GABAergic interneurons (13,14), our results are compatible with increased firing of inhibitory neurons. And increased firing of inhibitory GABAergic neurons may lead to higher extracellular potassium concentrations, which could trigger CSD as the neurophysiological correlate of the migraine aura (11).

In summary, we add the ninth mutation L1624P to the spectrum of FHM3 mutations. The unusual earlier onset might at least partly be related to this novel mutation. The gain-of-function defects, including the unique persistent current appearing near the threshold, are consistent with the pathomechanisms underlying FHM3. Here, we provide a detailed description of the novel L1624P mutation from the clinical, genetic and molecular points of view that will contribute to the understanding of the pathogenesis of the underlying migraine.

Article highlights

- Our studies identify a novel L1624P mutation in Na$_V$1.1 linked to pure familial hemiplegic migraine 3 (FHM3) with a remarkably early age of onset.
- Our gain-of-function results, including the unique threshold-near persistent current, are consistent with hyperexcitability of inhibitory interneurons, which, by means of increasing extracellular potassium, may facilitate cortical spreading depression (CSD).

References

1. Thomsen LL, Eriksen MK, Roemer SF, et al. A population-based study of familial hemiplegic migraine suggests revised diagnostic criteria. *Brain* 2002; 125: 1379–1391.

2. Headache Classification Committee of the International Headache Society (IHS). The International Classification of Headache Disorders, 3rd edition (beta version). *Cephalalgia* 2013; 33: 629–808.

3. Ophoff RA, Terwindt GM, Vergouwe MN, et al. Familial hemiplegic migraine and episodic ataxia type-2 are caused by mutations in the Ca^{2+} channel gene *CACNL1A4*. *Cell* 1996; 87: 543–552.

4. De Fusco M, Marconi R, Silvestri L, et al. Haploinsufficiency of *ATP1A2* encoding the Na$^+$/K$^+$ pump alpha2 subunit associated with familial hemiplegic migraine type 2. *Nat Genet* 2003; 33: 192–196.

5. Dichgans M, Freilinger T, Eckstein G, et al. Mutation in the neuronal voltage-gated sodium channel *SCN1A* in familial hemiplegic migraine. *Lancet* 2005; 366: 371–377.

6. Riant F, Roze E, Barbance C, et al. *PRRT2* mutations cause hemiplegic migraine. *Neurology* 2012; 79: 2122–2124.

7. Lauritzen M. Pathophysiology of the migraine aura. *Brain* 1994; 117: 199–210.

8. De Vries B, Frants RR, Ferrari MD, et al. Molecular genetics of migraine. *Hum Genet* 2009; 126: 115–132.

9. Silberstein SD and Dodick DW. Migraine genetics: Part II. *Headache* 2013; 53: 1218–1229.

10. Cestèle S, Scalmani P, Rusconi R, et al. Self-limited hyperexcitability: Functional effect of a familial hemiplegic migraine mutation of the Na$_V$1.1 (*SCN1A*) Na$^+$ channel. *J Neurosci* 2008; 28: 7273–7283.

11. Cestèle S, Schiavon E, Rusconi R, et al. Nonfunctional Na$_V$1.1 familial hemiplegic migraine mutant transformed into gain of function by partial rescue of folding defects. *Proc Natl Acad Sci U S A* 2013; 110: 17546–17551.

12. Meng H, Xu HQ, Yu L, et al. The *SCN1A* Mutation Database: Updating information and analysis of the relationships among genotype, functional alteration, and phenotype. *Hum Mutat* 2015; 36: 573–580.

13. Yu FH, Mantegazza M, Westenbroek RE, et al. Reduced sodium current in GABAergic interneurons in a mouse model of severe myoclonic epilepsy in infancy. *Nat Neurosci* 2006; 9: 1142–1149.

14. Ogiwara I, Miyamoto H, Morita N, et al. Na$_V$1.1 localizes to axons of parvalbumin-positive inhibitory interneurons: A circuit basis for epileptic seizures in mice carrying an Scn1a gene mutation. *J Neurosci* 2007; 27: 5903–5914.

15. Hedrich UB, Liautard C, Kirschenbaum D, et al. Impaired action potential initiation in GABAergic interneurons causes hyperexcitable networks in an epileptic mouse model carrying a human Na(V)1.1 mutation. *J Neurosci* 2014; 34: 14874–14889.

16. Oliva M, Berkovic SF and Petrou S. Sodium channels and the neurobiology of epilepsy. *Epilepsia* 2012; 53: 1849–1859.

17. Vanmolkot KR, Babini E, de Vries B, et al. The novel p.L1649Q mutation in the *SCN1A* epilepsy gene is associated with familial hemiplegic migraine: Genetic and functional studies. *Hum Mutat* 2007; 28: 522.

18. Weller CM, Pelzer N, de Vries B, et al. Two novel *SCN1A* mutations identified in families with familial hemiplegic migraine. *Cephalalgia* 2014; 34: 1062–1069.

19. Vahedi K, Depienne C, Le Fort D, et al. Elicited repetitive daily blindness: A new phenotype associated with hemiplegic migraine and *SCN1A* mutations. *Neurology* 2009; 72: 1178–1183.

20. Castro MJ, Stam AH, Lemos C, et al. First mutation in the voltage-gated Na$_V$1.1 subunit gene *SCN1A* with co-occurring familial hemiplegic migraine and epilepsy. *Cephalalgia* 2009; 29: 308–313.

21. Cestèle S, Labate A, Rusconi R, et al. Divergent effects of the T1174S *SCN1A* mutation associated with seizures and hemiplegic migraine. *Epilepsia* 2013; 54: 927–935.

22. Kahlig KM, Rhodes TH, Pusch M, et al. Divergent sodium channel defects in familial hemiplegic migraine. *Proc Natl Acad Sci U S A* 2008; 105: 9799–9804.

23. Lossin C, Wang DW, Rhodes TH, et al. Molecular basis of an inherited epilepsy. *Neuron* 2002; 34: 877–884.

24. Russell MB and Ducros A. Sporadic and familial hemiplegic migraine: Pathophysiological mechanisms, clinical characteristics, diagnosis, and management. *Lancet Neurol* 2011; 10: 457–470.

25. Freilinger T, Bohe M, Wegener B, et al. Expansion of the phenotypic spectrum of the *CACNA1A* T666M mutation: A family with familial hemiplegic migraine type 1, cerebellar atrophy and mental retardation. *Cephalalgia* 2008; 28: 403–407.

26. Jurkat-Rott K, Freilinger T, Dreier JP, et al. Variability of familial hemiplegic migraine with novel A1A2 Na+/K+-ATPase variants. *Neurology* 2004; 62: 1857–1861.

27. Fujiwara T, Sugawara T, Mazaki-Miyazaki E, et al. Mutations of sodium channel α subunit type 1 (*SCN1A*) in intractable childhood epilepsies with frequent generalized tonic-clonic seizures. *Brain* 2003; 126: 531–546.

28. Herini ES, Gunadi F, Van Kempen MJ, et al. Novel *SCN1A* mutations in Indonesian patients with severe myoclonic epilepsy in infancy. *Pediatr Int* 2010; 52: 234–239.

29. Marini C, Mei D, Temudo T, et al. Idiopathic epilepsies with seizures precipitated by fever and *SCN1A* abnormalities. *Epilepsia* 2007; 48: 1678–1685.

30. Mulley JC, Scheffer IE, Petrou S, et al. *SCN1A* mutations and epilepsy. *Hum Mutat* 2005; 25: 535–542.

31. Monné M, Nilsson I, Elofsson A, et al. Turns in transmembrane helices: Determination of the minimal length of a "helical hairpin" and derivation of a fine-grained turn propensity scale. *J Mol Biol* 1999; 293: 807–814.

32. Zhao Y, Scheuer T and Catterall WA. Reversed voltage-dependent gating of a bacterial sodium channel with proline substitutions in the S6 transmembrane segment. *Proc Natl Acad Sci U S A* 2004; 101: 17873–17878.

33. Cannon SC, Hayward LJ, Beech J, et al. Sodium channel inactivation is impaired in equine hyperkalemic periodic paralysis. *J Neurophysiol* 1995; 73: 1892–1899.